

Dalton Transactions

Accepted Manuscript



This is an *Accepted Manuscript*, which has been through the Royal Society of Chemistry peer review process and has been accepted for publication.

Accepted Manuscripts are published online shortly after acceptance, before technical editing, formatting and proof reading. Using this free service, authors can make their results available to the community, in citable form, before we publish the edited article. We will replace this *Accepted Manuscript* with the edited and formatted *Advance Article* as soon as it is available.

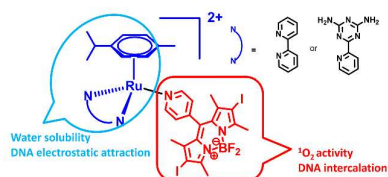
You can find more information about *Accepted Manuscripts* in the [Information for Authors](#).

Please note that technical editing may introduce minor changes to the text and/or graphics, which may alter content. The journal's standard [Terms & Conditions](#) and the [Ethical guidelines](#) still apply. In no event shall the Royal Society of Chemistry be held responsible for any errors or omissions in this *Accepted Manuscript* or any consequences arising from the use of any information it contains.

The BODIPY (boron dipyrromethene) derivatives and Ru(II) complexes are two types of functional compounds that have found wide applications in the fields of biology and medicine. We herein synthesized two new Ru(II) arene complexes based on an iodized BODIPY-containing pyridine (py-I-BODIPY) ligand, $[(p\text{-cym})\text{Ru}(\text{bpy})(\text{py-I-BODIPY})]^{2+}$ (2) and $[(p\text{-cym})\text{Ru}(2\text{-pydaT})(\text{py-I-BODIPY})]^{2+}$ (3), where *p-cym* = *para*-cymene, bpy = 2,2'-bipyridine, and 2-pydaT = 2,4-diamino-6-(2-pyridyl)-1,3,5-triazine. The photophysical, photochemical and photobiological properties of 2 and 3 were compared to that of $[(p\text{-cym})\text{Ru}(\text{bpy})(\text{py-BODIPY})]^{2+}$ (1). While 1 undergoes an efficient monodentate ligand dissociation upon visible light irradiation and therefore may photobind DNA as a potential photoactivated chemotherapy (PACT) agent, 2 and 3 can generate $^1\text{O}_2$ effectively and thus may serve as photosensitizers in photodynamic therapy (PDT). In electrophoresis experiments, 2 and 3 are even able to retard mobility of plasmid DNA in the dark at high concentrations. More importantly, the cytotoxicities of 2 and 3 against human ovarian adenocarcinoma SKOV3 cells are enhanced by about ten times under irradiation, leading to cytotoxicities more than one order of magnitude higher than that of cisplatin, demonstrating an efficient hybridization of the iodized BODIPY chromophore and the Ru(II) arene complex.

Two novel BODIPY-Ru(II) arene dyads enabling effective photo-inactivation against cancer cells

Hybrids of an iodized BODIPY chromophore and a Ru(II) arene complex leads to novel photoactivated anticancer agents with IC_{50} values of one order of magnitude lower than cisplatin against human ovarian adenocarcinoma SKOV3 cells.





Two novel BODIPY-Ru(II) arene dyads enabling effective photo-inactivation against cancer cells

Tianji Wang,^{a, b} Yuanjun Hou,^a Yongjie Chen,^{a, b} Ke Li,^{a, b} Xuexin Cheng,^a Qianxiong Zhou,^{*a} Xuesong Wang^{*a}

Received 00th January 20xx,
Accepted 00th January 20xx

DOI: 10.1039/x0xx00000x

www.rsc.org/

The BODIPY (boron dipyrromethene) derivatives and Ru(II) complexes are two types of functional compounds that have found wide applications in the fields of biology and medicine. We herein synthesized two new Ru(II) arene complexes based on an iodized BODIPY-containing pyridine (py-I-BODIPY) ligand, [(*p*-cym)Ru(bpy)(py-I-BODIPY)]²⁺ (**2**) and [(*p*-cym)Ru(2-pydaT)(py-I-BODIPY)]²⁺ (**3**), where *p*-cym = *para*-cymene, bpy = 2,2'-bipyridine, and 2-pydaT = 2,4-diamino-6-(2-pyridyl)-1,3,5-triazine. The photophysical, photochemical and photobiological properties of **2** and **3** were compared to that of [(*p*-cym)Ru(bpy)(py-BODIPY)]²⁺ (**1**). While **1** undergoes an efficient monodentate ligand dissociation upon visible light irradiation and therefore may photobind DNA as a potential photoactivated chemotherapy (PACT) agent, **2** and **3** can generate ¹O₂ effectively and thus may serve as photosensitizers in photodynamic therapy (PDT). In electrophoresis experiments, **2** and **3** are even able to retard mobility of plasmid DNA in the dark at high concentrations. More importantly, the cytotoxicities of **2** and **3** against human ovarian adenocarcinoma SKOV3 cells are enhanced by about ten times under irradiation, leading to cytotoxicities more than one order of magnitude higher than that of cisplatin, demonstrating an efficient hybridization of the iodized BODIPY chromophore and the Ru(II) arene complex.

Introduction

As a fascinating class of organic dyes, the BODIPY (boron dipyrromethene) derivatives have found wide applications in biological and medical fields, such as biological labeling, optical imaging, and fluorescent sensing, by virtue of their intense absorption profile in visible and near-IR region, unique narrow emission with high quantum yield, as well as excellent thermal and photochemical stability.¹ Not only versatile in diagnostic aspect, the BODIPY derivatives also display promising potential as therapeutic agents in photodynamic therapy (PDT).² As a type of non-invasive cancer treatment modality, PDT uses reactive oxygen species (ROS), mainly singlet oxygen (¹O₂), to inactivate tumor cells and tissues, while ¹O₂ are generated via energy transfer from the triplet excited state of a photosensitizer to oxygen.³ The spatial and temporal control on light irradiation renders PDT highly selective toward tumor tissues. For such application, a BODIPY dye should have a high intersystem crossing (ISC) efficiency to reach the triplet excited states effectively. The presence of heavy atoms (the so called heavy atom effect) will improve ISC efficiency remarkably, which has been fully utilized to boost the ISC efficiencies of the

BODIPY derivatives, and iodization is quite simple but very effective.⁴

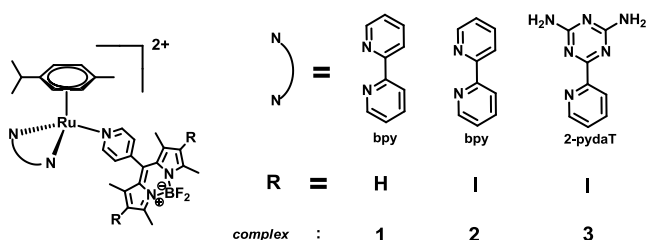
Compared to organic chromophores, transition metal complexes construct another big family of biological tools and medicinal agents.⁵ Among them, cisplatin, an anticancer drug that has been clinically used for decades, may serve as the most famous representative. While great efforts have been devoted to new Pt-based metallodrugs in hope of overcoming the severe side effects and intrinsic or acquired resistance associated with cisplatin,⁶ ruthenium complexes are drawing growing attention in the development of new anticancer drugs due to their rich and tunable chemical, photophysical and photochemical properties.⁵ For example, NAMI-A and KP101, both Ru(III)-based complexes, have reached phase I/II clinical trials.^{5b} Moreover, many Ru complexes exhibit high ¹O₂ quantum yields and therefore are attractive in PDT.⁷ In recent years, the Ru complexes comprising photolabile ligand(s) have also been studied extensively as photoactivated chemotherapy (PACT) agents.^{5b, 5e, 8} After photoinduced ligand dissociation, the *in-situ* formed coordination-unsaturated Ru residue may covalently bind DNA in a manner very similar to cisplatin. It is worth noting that, for some Ru(II) arene complexes, photoinduced ligand dissociation may lead to monofunctional coordination of the resultant Ru fragment toward DNA.^{8d, e, i} Similar to PDT, PACT is also expected to be more selective than traditional chemotherapy due to the use of irradiation as the trigger of drug activity.

Both organic chromophores and transition metal complexes have their own strengths and weaknesses as therapeutic

^a Key Laboratory of Photochemical Conversion and Optoelectronic Materials, Technical Institute of Physics and Chemistry, Chinese Academy of Sciences, Beijing 100190, P. R. China. E-mail: xswang@mail.ipc.ac.cn, zhouqianxiong@mail.ipc.ac.cn

^b Graduate School of Chinese Academy of Sciences, Beijing 100049, P. R. China.

agents, and the hybridization of them often leads to surprising properties that cannot be obtained in each single component.⁹ As an example, the incorporation of a BODIPY skeleton into a ligand of a transition metal complex can open many new energy or electron transfer pathways between them, exhibiting potentials in light harvesting, energy storage, and sensor.¹⁰ We recently synthesized a BODIPY-modified pyridine ligand (py-BODIPY in Scheme 1) and its Ru arene complex, $[(p\text{-cym})\text{Ru}(\text{bpy})(\text{py-BODIPY})]^{2+}$, (**1** in Scheme 1, *p-cym* = *para*-cymene, *bpy* = 2,2'-bipyridine) for PACT application.¹¹ The photoinduced intramolecular electron transfer from py-BODIPY to Ru moiety gives rise to efficient monodentate ligand dissociation, meanwhile the photoactivation wavelength is extended from UV region to 504 nm with one order of magnitude enhancement in extinction coefficient than general Ru complexes.¹¹ We surmised that the iodization of py-BODIPY (py-I-BODIPY in Scheme 1) may further offer the corresponding complex $^1\text{O}_2$ generation ability and thus PDT activity. Bearing these in mind, $[(p\text{-cym})\text{Ru}(\text{bpy})(\text{py-I-BODIPY})]^{2+}$ and $[(p\text{-cym})\text{Ru}(2\text{-pydaT})(\text{py-I-BODIPY})]^{2+}$ (**2** and **3** in Scheme 1, 2-pydaT = 2,4-diamino-6-(2-pyridyl)-1,3,5-triazine) were prepared and their photophysical, photochemical, and photobiological properties were investigated using **1** as a control. Both **2** and **3** photo-inactivated human ovarian adenocarcinoma SKOV3 cells more efficiently than **1**. Additionally, **2** and **3** photocleaved DNA, while **1** covalently bound DNA upon irradiation. More interestingly, **2** and **3** are able to retard DNA mobility even in the dark. These dramatic disparities are discussed, and the underlying mechanisms may provide guidelines for further optimization of such type of BODIPY-transition metal complex hybrids for their photo-activated anticancer applications.



Scheme 1. Chemical structures of the complexes 1-3.

Results and Discussion

Photophysical property

Table 1 collects the basic photophysical properties of **1-3** and the corresponding monodentate ligands in CH_3CN and PBS (pH = 7.4, 5 mM)/DMSO (8:1), and the absorption and emission spectra of **1** and **2** in CH_3CN are shown in Figure 1. Our previous work has demonstrated that the absorption spectrum of **1** is the superposition of those of $[(p\text{-cym})\text{Ru}(\text{bpy})(\text{py})]^{2+}$ and py-BODIPY, and the intense visible absorption band originates from py-BODIPY.¹¹ Similar results were also observed in the absorption spectra of **2** and **3**. Compared to py-BODIPY, the absorption maximum of py-I-BODIPY has a red shift of ca. 35 nm as the result

of the iodization. This spectrum red shift retains in **2** and **3** and is expected to be beneficial for in vivo photoactivation since light of longer wavelength will penetrate deeper in tissue.

Similar to absorption spectra, iodization-induced red shift was also observed in the emission spectra. Notably, due to the presence of heavy atom effect, the fluorescence quantum yields undergo a decrease from 0.21 (in CH_3CN) for py-BODIPY to 0.13 (in CH_3CN) for py-I-BODIPY. Upon coordination onto the Ru center, the fluorescence quantum yields of both monodentate ligands experience a marked reduction, e.g. from 0.21 to 0.06 for **1** and from 0.13 to 0.04 for **2**. This quenching effect in **1** has been ascribed to the intramolecular photoinduced electron transfer from py-BODIPY to the Ru(II) arene moiety, which leads to a cationic py-BODIPY, accounting for its efficient photodissociation.¹¹ Such electron transfer process is expected to occur in **2** and **3**, but with a diminished efficiency (see discussion below). Additionally, the Ru atom may also exert heavy atom effect to the monodentate ligand coordinated onto it.

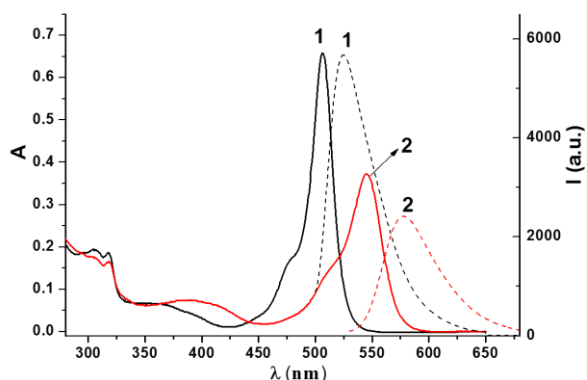


Figure 1. UV-Vis absorption and emission spectra of **1** and **2** (10 μM) in PBS (pH = 7.4, 5 mM)/DMSO (8:1) (λ_{ex} are 470 and 500 nm for **1** and **2**, respectively).

Table 1. Photophysical properties of **1-3**, py-BODIPY and py-I-BODIPY.

compound	solvent	$\lambda_{\text{max abs}}$ (nm)	ϵ ($\text{M}^{-1}\text{cm}^{-1}$)	$\lambda_{\text{max em}}$ (nm)	Φ_{F}
py-BODIPY	CH_3CN	500	99800	518	0.21 ^a
	PBS:DMSO(1:1)	503	82400	529	0.05
py-I-BODIPY	CH_3CN	534	66500	558	0.13
	PBS:DMSO(1:1)	538	53200	565	0.03
1	CH_3CN	504	62400	521	0.06 ^a
	PBS:DMSO(8:1)	507	65800	529	0.05
2	CH_3CN	542	40100	574	0.04
	PBS:DMSO(8:1)	545	37200	578	0.03
3	CH_3CN	540	39900	568	0.04
	PBS:DMSO(8:1)	543	36300	573	0.03

^a ref 11.

From CH_3CN to PBS, the absorption and emission spectra of **1-3**, py-BODIPY and py-I-BODIPY have a slight red shift (Table 1). In

contrast, the fluorescence quantum yields of py-BODIPY and py-I-BODIPY decrease significantly. This may be due to their poor water solubility, leading to aggregation and fluorescence quenching. The dynamic-light-scattering (DLS) experiments support our explanation (Figure S1). In PBS/DMSO (8:1) solutions of py-BODIPY and py-I-BODIPY (5 μM), particles with average diameter of 200 nm were determined, while no nanoparticles were observed in their solutions in CH_3CN . For **1-3**, the fluorescence quenching in PBS (pH = 7.4, 5 mM)/DMSO (8:1) are far less important than py-BODIPY and py-I-BODIPY. This finding is in good agreement with the oil/water partition coefficients, which follow the order of py-BODIPY \approx py-I-BODIPY \gg **3** $>$ **2** $>$ **1** (Table 2). The enhanced water solubility for **1-3** may result from the cationic character of the Ru arene moiety. Despite more hydrophilic than py-I-BODIPY, particles with diameter of 100 nm were still found in the PBS (pH = 7.4, 5 mM)/DMSO (8:1) solutions of **2** and **3** (Figure S1). Due to the presence of electrostatic repulsion between cationic **2** and **3**, loose particles and thus weak fluorescence quenching are expected for them.

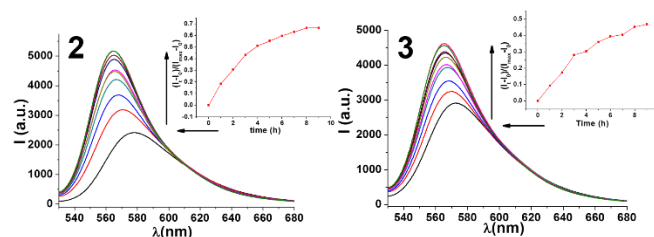


Figure 2. Fluorescence spectra changes of **2** and **3** (10 μM) in PBS (pH = 7.4, 5 mM)/DMSO (8:1) upon irradiation (> 470 nm). The insets show intensity variation at 565 nm as a function of irradiation time, where I_{max} , I_0 and I_t are, respectively, the fluorescence intensities of py-I-BODIPY (10 μM) in PBS/DMSO (8:1), **2** or **3** before and after irradiation for a period of time.

$^1\text{O}_2$ generation

EPR measurements were at first carried out to qualitatively compare the $^1\text{O}_2$ generation abilities of **1-3**, using TEMP as spin-trapping agent. Upon irradiation with 532 nm laser, a three-line signal with hyperfine coupling constant of 16.0 G appeared in solutions of **2** and **3** in air-saturated CH_3CN (Figure 3), in line with the signal of TEMPO (adduct of TEMP and $^1\text{O}_2$).¹² Control experiments indicated that the complex, irradiation, and oxygen are all necessary for the signal. We also measured the absorption and emission spectra of the EPR samples before and after laser irradiation. No UV-Vis and emission spectra changes were observed, revealing that $^1\text{O}_2$ originates from **2** or **3** rather than the free py-I-BODIPY ligand dissociated from the complex. When the OD values of the samples at 532 nm were kept constant, the signal intensities reflect an order of py-I-BODIPY $>$ **2** \approx **3** in $^1\text{O}_2$ generation. In sharp contrast, the TEMPO signal intensity obtained in the cases of **1** and py-BODIPY are nearly the same as that in blank solution where TEMP was present only (Figure S2 and S3), suggesting their poor $^1\text{O}_2$ generation.

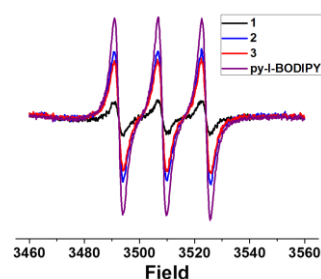


Figure 3. EPR signals obtained upon irradiation of air-saturated CH_3CN solutions of TEMP (1 mM) and **1**, **2**, **3** or py-I-BODIPY (10 μM) with 532 nm pulsed laser.

We then compared the $^1\text{O}_2$ generation abilities of **1-3**, py-BODIPY and py-I-BODIPY using a common chemical trapping method (Figure

Table 2. Oil/water partition coefficients, $^1\text{O}_2$ quantum yields and triplet excited state life times of **1-3**, py-BODIPY and py-I-BODIPY.

	1	2	3	py-BODIPY	py-I-BODIPY
$\text{Log } P_{\text{O}/\text{W}}^{\text{a}}$	0.84	0.97	1.18	2.81	2.78
$\Phi(^1\text{O}_2)^{\text{b}}$	0.05	0.68	0.63	0.04	0.73
$\tau_{\text{T}}/\mu\text{s}^{\text{b}}$	nd	0.95	1.08	nd	13.89

^a *n*-octanol/water partition coefficient; ^b in air-saturated CH_3CN .

Ligand photodissociation

Our previous study shows an almost full dissociation of the py-BODIPY ligand from **1** upon irradiation (> 470 nm) for only 9 min as evidenced by complete recovery of the fluorescence intensity of the free py-BODIPY.¹¹ However, the fluorescence intensity recovery was only 70% for **2** and 50% for **3** (insets of Figure 2) after 9 h of irradiation under the same condition. The nearly two orders of magnitude reduction in ligand photodissociation rates may be mainly due to the heavy atom effect from the iodine atoms, which leads to an efficient population of the py-I-BODIPY based triplet excited state. The driving force for the intramolecular electron transfer from py-BODIPY in its singlet excited state to the Ru arene moiety has been estimated to be -0.29 eV.¹¹ Moreover, the energy gap between the singlet excited states of py-BODIPY and py-I-BODIPY is calculated to be 0.22 eV (based on the emission red shift from 521 nm for **1** to 574 nm for **2**). It is clear that the electron transfer from the triplet excited state of py-I-BODIPY to the Ru arene moiety will be a thermodynamically unfavorable process. Thus, the observed slow ligand photodissociation of **2** and **3** should originate from the electron transfer of the singlet excited state of py-I-BODIPY, which has a minor population and a very small driving force of -0.07 eV.

4), in which DPBF is allowed to react with $^1\text{O}_2$ and its fluorescence bleaching rate may serve as a measure on the quantity of $^1\text{O}_2$.¹³ Taking $[\text{Ru}(\text{bpy})_3]^{2+}$ as the standard ($\Phi_{\Delta} = 0.57$ in CH_3CN),¹⁴ the $^1\text{O}_2$ quantum yields were measured to be 0.73 for py-I-BODIPY, 0.68 for **2**, 0.63 for **3**, 0.05 for **1** and 0.04 for py-BODIPY (Table 2), consistent very well with the EPR experimental results.

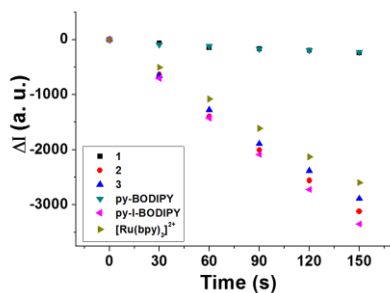


Figure 4. DPBF fluorescence bleaching ($\lambda_{\text{em}} = 479$ nm, $\lambda_{\text{ex}} = 440$ nm) in air-saturated CH_3CN upon irradiation at 512 nm in the presence of **1-3**, py-BODIPY or py-I-BODIPY.

Additionally, the time-resolved absorption spectra were determined to better understand the behaviors of **1-3**, py-BODIPY and py-I-BODIPY in $^1\text{O}_2$ generation. No signals were obtained for **1** and py-BODIPY in the time span of ns to μs , hinting at a process of major singlet excited state in nature, which is in line with their poor $^1\text{O}_2$ generation. In the cases of **2**, **3** and py-I-BODIPY, transient absorption spectra with similar profile as shown in Figure 5 were observed, indicating the triplet excited state of py-I-BODIPY is the lowest-lying in both **2** and **3**. The T-T absorption lifetimes are, respectively, 0.95 μs for **2**, 1.08 μs for **3**, and 13.89 μs for py-I-BODIPY, accounting for their efficient $^1\text{O}_2$ generation. The shorter lifetimes for **2** and **3** may be the result of the heavy atom effect from the Ru center.

Interestingly, Zhao and coworkers reported a triplet excited state lifetime of 57 μs for another diiodo-BODIPY derivative, in which the substituent at *meso*-position of the I-BODIPY skeleton is phenyl rather than pyridyl group.¹⁵ The short lifetime of 13.89 μs for py-I-BODIPY might suggest an intramolecular electron transfer process from I-BODIPY to py group which speeds up the decay of the triplet excited state.

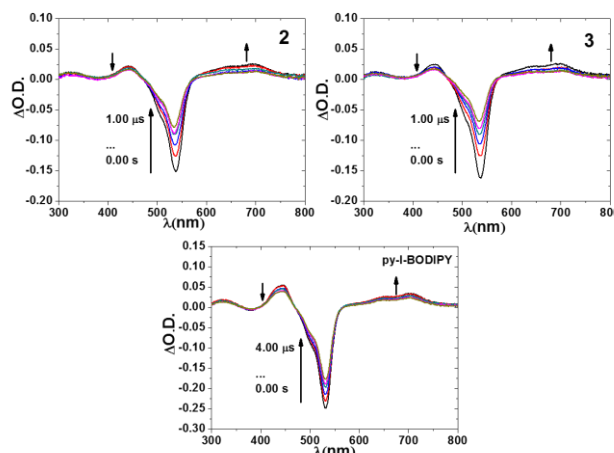


Figure 5. T-T absorption spectra of **2**, **3** and py-I-BODIPY in Ar-saturated CH_3CN .

DNA binding and cleavage

In anticancer therapies, including PDT and PACT, DNA is one of the primary biotargets. The studies on the interactions between drugs and DNA are important and helpful in understanding the anticancer mechanisms. In our experiments, the DNA interaction behaviors of **1-3** were examined at first in the dark. As shown in Figure 6, the titration of CT-DNA led to a significant absorbance reduction, accompanying a noticeable spectrum red shift, a typical behavior for common DNA intercalators. In our previous work, a series of BODIPY derivatives were also found to bind DNA in a manner of intercalation.^{4b} The π - π stacking between the intercalating chromophore and the DNA base pairs is believed to be responsible for the bathochromic shift and hypochromic effect.¹⁶ The binding constants were determined to be $2.52 \times 10^6 \text{ M}^{-1}$ for **1**, $5.19 \times 10^6 \text{ M}^{-1}$ for **2**, and $1.40 \times 10^6 \text{ M}^{-1}$ for **3**. The binding strength of **2** is twice that of **1**, presumably due to the larger conjugation structure of py-I-BODIPY than py-BODIPY and thus stronger π - π staking. The nearly four times lower binding constant of **3** than **2** demonstrates that bidentate ligands of bpy and 2-pydaT also play an important role. Additionally, the interaction between DNA and py-BODIPY or py-I-BODIPY is negligible, probably due to the lack of positive charge for both ligands. The strong hydrophobicity of both ligands, evidence by forming nanoparticles in PBS/DMSO (8:1), may also restrict their binding to DNA. Additionally, we examined the UV-vis absorption and CD spectra of CT-DNA in PBS and PBS/DMSO (8:1). Negligible spectra changes were found, suggesting that DNA remained its own structure in our experimental conditions.

We then examined the influences of **1-3**, py-BODIPY, and py-I-BODIPY on the electrophoresis of DNA in the presence of irradiation (> 470 nm). As expected, at concentration of 10 μM , both py-BODIPY (Lane 6 and 7 in Figure S4) and py-I-BODIPY (Lane 5 and 6 in Figure 7) had no detectable effect on the electrophoresis of supercoiled pUC19 plasmid DNA irrespective of irradiation, in good agreement with their negligible interaction with CT-DNA in the

dark. Though py-I-BODIPY can generate $^1\text{O}_2$, no DNA cleavage was observed (*i.e.* no appearance of nicked circular (NC) or linear form of pUC19 DNA), due to the short lifetime, low apparent diffusion coefficient and thus limited sphere of activity of $^1\text{O}_2$.¹⁷ Interestingly, **1** has no effect at 10 μM even upon irradiation (Lane 2 and 3 in Figure 7). Thus, we examined its interaction with pUC19 DNA at elevated concentrations (Figure S5). At 25 μM or higher concentrations, **1** was able to retard the mobility of supercoiled (SC) pUC19 DNA effectively upon irradiation (Lane 5-7 in Figure S5). This may be attributed to the covalent binding of **1** to DNA after the photodissociation of the monodentate ligand.⁸

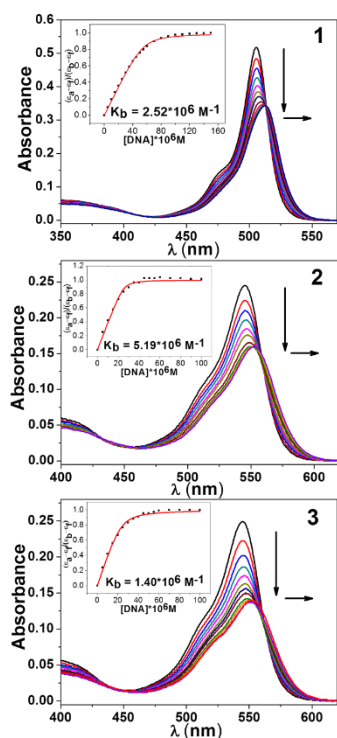


Figure 6. Absorption spectra changes of **1**, **2** and **3** (5 μM) in PBS (pH = 7.4, 5 mM)/DMSO (8:1) upon CT-DNA titration.

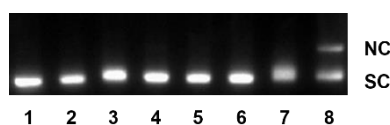


Figure 7. Agarose gel electrophoresis pattern of supercoiled pUC19 plasmid DNA (40 $\mu\text{g}/\text{mL}$) in air-saturated PBS (pH = 7.4, 5 mM)/DMSO (8:1) under different conditions. Lane 1, DNA + hv; Lane 2, DNA + **1**; Lane 3, DNA + **1** + hv; Lane 4, DNA alone; Lane 5, DNA + py-I-BODIPY; Lane 6, DNA + py-I-BODIPY + hv; Lane 7, DNA + **2**; Lane 8, DNA + **2** + hv. hv denotes an irradiation (> 470 nm) for 15 min. SC and NC represent supercoiled circular and nicked circular forms, respectively. The concentrations of **1**, **2** and py-I-BODIPY are 10 μM .

Different to **1**, **2** and **3** can photocleave DNA at 10 μM as evidenced by the transformation of pUC19 DNA from SC to NC form (Lane 7 and 8 in Figure 7 and Lane 3 and 4 in Figure S4). Control experiments revealed that the DNA photocleavage was restricted significantly in the presence of NaN_3 (Lane 2 and 3 in Figure S6), an effective scavenger of $^1\text{O}_2$. In contrast, the scavengers of hydroxyl radical (DMSO) and H_2O_2 (catalase) had negligible influences (Lane 4 and 5 in Figure S6). Obviously, the DNA photocleavage by **2** and **3** stems from $^1\text{O}_2$ generation.

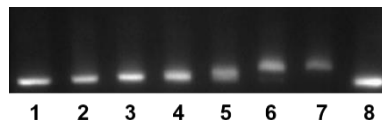


Figure 8. Agarose gel electrophoresis pattern of supercoiled pUC19 plasmid DNA (40 $\mu\text{g}/\text{mL}$) in air-saturated PBS (pH = 7.4, 5 mM)/DMSO (8:1) in the dark and in the presence of varied concentrations of **2**. Lane 1 and 8, DNA alone; Lane 2-7, the concentrations of **2** are 1, 5, 10, 25, 50, and 100 μM , respectively.

It is worth noting that **2** led to a discernible bleaching and somewhat mobility retardation on the SC band at 10 μM in the dark (Lane 7 in Figure 7). At elevated concentrations, such effect became more remarkable as shown in Figure 8. **3** displayed a very similar behavior (Figure S7). We tentatively assign the phenomena to the aggregation of **2** and **3** in aqueous solutions at higher concentrations due to their limited water solubility (Table 2). DLS measurements proved the formation of nanoparticles (Figure S1) in PBS/DMSO (8:1) solutions of **2**, **3**, and py-I-BODIPY. Different to the nanoparticles of py-I-BODIPY, the nanoparticles of **2** and **3** are expected to be highly positively charged, favoring electrostatic interaction with highly negatively charged DNA and refraining their separation by the electric field applied in electrophoresis. Recently, several Ru complexes bearing multiple positive charges were found to be able to retard DNA mobility and even condense DNA effectively.¹⁸

Cytotoxicity

The DNA photobinding ability of **1** and the DNA photocleavage abilities of **2** and **3** encouraged us to examine their phototoxicity against cancer cells. Human ovarian adenocarcinoma SKOV3 cells were used as model and cell viability was assayed by MTT method using cisplatin as a control. Cells were incubated with the Ru complexes for 4 h in the dark, then subjected to light irradiation (> 470 nm) for 15 min, and finally incubated in the dark for another 20 h. Dark toxicity measurements were run in parallel. The mixed solvent of DMEM/DMSO (8:1) has negligible cytotoxicity toward SKOV3 cell. As shown in Figure 9, the cytotoxicities of **2** and **3** under irradiation are more than one order of magnitude higher than that of cisplatin. For example, the cell viability declined to 2.2% at 1 μM of **2**. In contrast, the cell viability decreased to 36.3% at 1 μM of cisplatin. More importantly, the photoinduced toxicity enhancement index (PI) values of both complexes are as high as around 10, showing promising potentials as PDT agents. In contrast, the PI value of **1** is only 1.4. Though ligand photodissociation of **1** may occur efficiently, the DNA photobinding activity of **1** is quite

poor at lower concentrations (Lane 3 in Figure 7), which might be responsible for its disappointing photoactivation property. On the other hand, the poor photoactivation behavior of **1** vindicates that the potent photoactivated anticancer abilities of **2** and **3** result unambiguously from their $^1\text{O}_2$ activities, since **2** and **3** are far less efficient than **1** in ligand photodissociation.

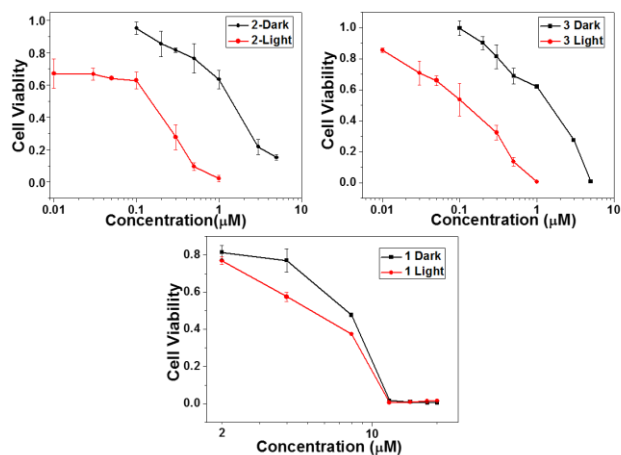


Figure 9. Cytotoxicities of **1-3** against SKOV3 cells in the dark or under irradiation ($\lambda > 470$ nm) for 15 min.

The attractive photoactivated anticancer properties of **2** and **3** clearly have had the benefits from both py-I-BODIPY and the Ru(II) arene moieties. The former renders **2** and **3** a high $^1\text{O}_2$ quantum yield and DNA intercalation ability, while the latter endows **2** and **3** with proper hydrophobic-hydrophilic balance as well as strong electrostatic interaction with DNA.

By monitoring the characteristic absorption of py-BODIPY and py-I-BODIPY of the complex-treated SKOV3 cells, the cellular uptake amounts were measured to be 284 ± 16 pmol/ 10^6 cells for **1**, 306 ± 13 pmol/ 10^6 cells for **2** and 303 ± 12 pmol/ 10^6 cells for **3**, respectively, after 4 h incubation at the complex concentration of 1 μM . Because the three complexes showed similar cellular uptake abilities, their disparities in phototoxicity should originate from other factors, e.g. $^1\text{O}_2$ generation and subcellular localization.

We also characterized the cellular uptake and subcellular localization of **2** and **3** using fluorescence imaging technique as both of them are weakly emissive. Fluorescence confocal micrographs (Figure S8 and S9) show that **2** and **3** can be taken up by SKOV3 cells and scatter throughout the cytoplasm. Double-stain experiments indicate that **2** may enter mitochondria and endoplasmic reticulum (ER) while **3** localizes in ER preferentially. Both **2** and **3** cannot penetrate into nucleus. These results demonstrate the subtle role of bpy and 2-pydaT.

Conclusions

Two new Ru(II) arene/iodized BODIPY hybrids, the complexes **2** and **3**, were designed and synthesized and their properties were compared in detail with their analogue, the complex **1**, which has been reported in our previous work. Due to the heavy atom effect

from the iodine atoms, **2** and **3** display high $^1\text{O}_2$ quantum yields and can cleave DNA effectively upon visible light irradiation. In contrast, an efficient electron transfer from the singlet excited state of py-BODIPY to the Ru(II) arene moiety occurs in **1**, which leads to a fast dissociation of py-BODIPY from the Ru(II) center and allows for covalent binding of the resultant Ru residue to DNA. Though **1**, **2**, and **3** are expected to be potential candidates in PACT and PDT applications, *in vitro* experiments reveal that **2** and **3** may photoinactivate human ovarian adenocarcinoma SKOV3 cells in a far higher efficacy than **1**. The attractive PDT activities of **2** and **3** are obviously the result of the integration of both iodized BODIPY and the Ru(II) arene moieties. The former provides **2** and **3** with potent $^1\text{O}_2$ activity and strong DNA intercalating ability, and the latter offer the complexes suitable water solubility and additional electrostatic interaction with DNA. Our work demonstrates a promising strategy to fully make use of the merits of different types of chromophores in developing new generation of photoactivated anticancer drugs.

Experimental Section

Materials: 2,4-Dimethylpyrrole, 4-benzaldehyde, 2,3-dichloro-5,6-dicyano-1,4-benzoquinone, iodine, iodic acid, boron trifluoride diethyl etherate ($\text{BF}_3 \cdot \text{Et}_2\text{O}$, 98%), NH_4PF_6 , 2, 2'-bipyridine, 2-cyanopyridine, dicyandiamide, methyl cellosolve and $[[(\eta^6\text{-}p\text{-cymene})\text{RuCl}(\mu\text{-Cl})_2]$ were purchased from Sigma-Aldrich. Methanol, dichloromethane, triethylamine and acetonitrile were redistilled prior to use.

Syntheses: The ligands of 2-pydaT and py-BODIPY were prepared with reported methods.^{11, 19} And the ligand of py-I-BODIPY was obtained upon iodination of py-BODIPY by iodine and iodic acid using a reported procedure.²⁰ Following the synthetic routes of complex **1**,¹¹ the complexes **2** and **3** were prepared and characterized.

py-I-BODIPY. Yield, 98%. ^1H NMR (400 MHz, in CD_3COCD_3): δ = 1.47 (s, 6H), 2.61 (s, 6H), 7.58–7.59 (d, 2H, J = 6.0 Hz), 8.86–8.88 (d, 2H, J = 5.9 Hz). HR ESI-MS: Calcd for $\text{C}_{18}\text{H}_{16}\text{BF}_2\text{N}_3\text{I}_2$: m/z = 576.9495. Found: m/z = 576.9607.

[(*p*-cym)Ru(bpy)(py-I-BODIPY)](PF₆)₂ (complex **2).** Yield, 25%. ^1H NMR (400 MHz, in CD_3COCD_3): δ = 1.10–1.14 (m, 12H), 2.23 (s, 3H), 2.57 (s, 6H), 2.79–2.81 (m, 1H), 6.61–6.62 (d, 2H, J = 6.5 Hz), 6.97–6.99 (d, 2H, J = 6.5 Hz), 7.80–7.81 (d, 2H, J = 6.5 Hz), 8.10–8.13 (t, 2H, J = 6.7 Hz), 8.51–8.55 (t, 2H, J = 7.9 Hz), 8.71–8.75 (d, 2H, J = 8.0 Hz), 9.03–9.05 (d, 2H, J = 6.5 Hz), 10.24–10.25 (d, 2H, J = 5.7 Hz). HR ESI-MS: Calcd for $(\text{C}_{38}\text{H}_{38}\text{BF}_2\text{N}_5\text{I}_2\text{Ru})^{2+}$ ($\text{M}-2\text{PF}_6$)²⁺: m/z = 484.2142. Found: m/z = 484.2135 ($\text{M}-2\text{PF}_6$)²⁺. Anal. calcd for $\text{C}_{38}\text{H}_{38}\text{BF}_{14}\text{N}_5\text{P}_2\text{I}_2\text{Ru} \cdot 2\text{H}_2\text{O}$: C, 40.34; H, 3.56; N, 6.19. Found: C, 40.22; H, 3.51; N, 6.18.

[(*p*-cym)Ru(2-pydaT)(py-I-BODIPY)](PF₆)₂ (complex **3).** Yield, 21%. ^1H NMR (400 MHz, in CD_3COCD_3): δ = 1.17–1.18 (d, 6H, J = 5.9 Hz), 1.24 (s, 6H), 2.03–2.05 (m, 1H), 2.44 (s, 3H), 2.95 (s, 6H), 6.63–6.65 (d, 2H, J = 6.5 Hz), 7.09–7.10 (d, 2H, J = 6.5 Hz), 7.97–7.98 (d, 2H, J = 6.5 Hz), 8.42–8.45 (t, 2H, J = 6.8 Hz), 8.79–8.83 (t, 2H, J = 8.0 Hz), 8.96–9.01 (m, 4H), 10.24–10.25 (d, 2H, J = 5.7 Hz). HR ESI-MS: Calcd for $(\text{C}_{36}\text{H}_{38}\text{BF}_2\text{N}_9\text{I}_2\text{Ru})^{2+}$ ($\text{M}-2\text{PF}_6$)²⁺: m/z = 500.5222. Found: m/z = 500.5204 ($\text{M}-2\text{PF}_6$)²⁺. Anal. calcd for $\text{C}_{36}\text{H}_{38}\text{BF}_{14}\text{N}_9\text{P}_2\text{I}_2\text{Ru} \cdot 2\text{H}_2\text{O}$: C, 32.60; H, 3.19; N, 9.50. Found: C, 32.33; H, 3.10; N, 9.30.

Instruments and methods: ^1H NMR spectra were recorded on a Bruker DMX-400 MHz spectrophotometer, using SiMe_4 as standard. High resolution mass spectra were obtained on a Bruker APEX IV FT-MS. Elemental analysis was performed on an Elementar Vario EL instrument. UV-Vis spectra were recorded on a Shimadzu UV-

1601PC spectrophotometer. Fluorescence emission spectra were taken on a Hitachi F-4600 fluorescence spectrophotometer. DLS experiments were carried out at room temperature on a Malvern Zetasizer nanoZS instrument.

EPR spectra were obtained on a Bruker ESP-300E spectrometer at 9.8 GHz, X-band with 100 Hz field modulation, using TEMP as spin trapping agent. Samples were injected quantitatively into home-made quartz capillaries, then illuminated in the cavity of the EPR spectrometer with a Nd:YAG laser at 532 nm (5-6 ns of pulse width, 10 Hz of repetition frequency, 30 mJ/pulse energy).

Time-resolved absorption spectra were measured at room temperature on a LP920 laser flash photolysis setup (Edinburgh), using a computer-controlled Nd:YAG laser as the excitation light. The laser and analyzing light beam passed perpendicularly through a 1 cm quartz cell. The complete time-resolved spectra were obtained using a gated CCD camera (Andor iSTAR); the kinetic traces were detected by a Tektronix TDS 3012B oscilloscope and a R928P photomultiplier and analyzed by Edinburgh analytical software. All samples were degassed with high-purity argon for over 30 min before measurements.

Oil/water partition coefficient measurement: The *n*-octanol/water partition coefficients (Log $P_{o/w}$) were determined at room temperature following a reported method.²¹ Typically, solutions of each compound (10 μ M) in 1 mL PBS (pH = 7.4, 5 mM) and 1 mL *n*-octanol were sonicated for 30 min. After separation by centrifugation, the amounts of the compound in each phase were quantified by the absorbance of the examined compound at its absorption maximum. The results were the average of three independent measurements.

¹O₂ measurement: The reaction of ¹O₂ with DPBF was adopted to assess the ¹O₂ generation ability.¹³ A series of 2 mL of air-saturated CH₃CN solutions of DPBF and the examined compound, of which the absorbance at 512 nm was adjusted to the same, were illuminated with the light of 512 nm (obtained from a Hitachi F-4600 fluorescence spectrophotometer). The consumption of DPBF was followed by recording the emission spectra of DPBF.

DNA titration: All experiments involving DNA were performed in PBS (pH = 7.4, 5 mM)/DMSO (8:1). DNA solutions were obtained by dispersing the desired amount of DNA in PBS/DMSO and stirring overnight at temperature below 4 °C. The concentration of DNA was calculated using the extinction coefficient at 260 nm ($\epsilon = 6600 \text{ M}^{-1} \text{ cm}^{-1}$).

The DNA binding constants of the examined complexes were determined by monitoring the absorption spectra changes of the complexes with increasing the concentrations of CT-DNA. Non-linear fitting of eqn (1) and (2) to the experimental data yields the binding constant K_b .

$$(\epsilon_a - \epsilon_f)/(\epsilon_b - \epsilon_f) = (b - (b^2 - 2K_b^2 C_t [\text{DNA}]/s)^{1/2})/2K_b C_t \quad (1)$$

$$b = 1 + K_b C_t + K_b [\text{DNA}]/2s \quad (2)$$

where ϵ_f and ϵ_b represent the extinction coefficients at the absorption maxima of the free and bound complex, ϵ_a is the apparent extinction coefficient of the complex in the presence of CT-DNA, [DNA] denotes the concentration of CT-DNA in nuclear phosphate, C_t is the concentration of the complex, and s is the binding site size.

DNA electrophoresis: DNA photocleavage abilities of the examined compounds were evaluated using supercoiled pUC19 plasmid DNA as target. A 50 μ L solution of DNA (40 μ g/mL) and the examined compound (10 μ M) in PBS (pH = 7.4, 5 mM)/DMSO (8:1) was irradiated under an Oriel 91192 solar simulator equipped with a glass filter to cut off the light below 470 nm. After irradiation, 10 μ L gel loading buffer was added. A 10 μ L sample was taken for agarose gel electrophoresis at 80 V for 1.5 h. The gel was stained with EB (1 mg L⁻¹ in H₂O) for 0.5 h and then analyzed using a Gel Doc XR system (Bio-Rad).

Cytotoxicity assay: MTT assay was utilized to analyze cell viability. SKOV3 cells were plated at 2×10^5 per well in a Nunc 96 well plate and incubated for 24 h in 150 μ L DMEM medium at 37°C under 5% CO₂ atmosphere. Then, the cells were exposed to increasing concentrations of the examined compounds and incubated for 4 h at 37°C, and activated for 15 min with light > 470 nm (from an Oriel 91192 Solar simulator equipped with a long-pass filter) at 25°C. After another 20 h of incubation in the dark at 37°C, 10 μ L MTT (3-(4,5-dimethylthiazol-2-yl)-2,5-diphenyltetrazoliumbromide) solution in DMEM was added and the cells were maintained at 37°C for 4 h. Afterward, a mixed solution of CH₃OH/DMSO (1:1) was added and the absorbance at 595 nm was read on a Thermo MK3Multiscan microplate reader. The cell viability data are normalized to 100% viable (untreated) cells and are the average of at least three independent measurements at each dose.

Cell Stain: 1×10^5 SKOV3 cells in 2 mL DMEM medium were seeded on a coverslip and incubated overnight at 37 °C under 5% CO₂ atmosphere. The cells were incubated with a solution of **2** or **3** (0.5 μ M) in DMEM for 25 min and then 1.0 μ M of DAPI (Nucleus Probes), Mito-Tracker Red (Molecular Probes) or ER-Tracker Red (Molecular Probes) in DMEM for another 15 min at 37°C. After rinsed three times with PBS (pH = 7.4, 5 mM), the cells were viewed with a Nikon multiphoton microscope (A1R MP) equipped a 60 \times oil-immersion objective lens and living cell workstation. A 488 nm argon laser, a 561 nm helium neon laser and a 640 nm helium neon laser were used as light sources.

Cellular uptake: 5 mL of SKOV3 cells were seeded into flasks with bottom area of 25 cm² at a cell density of 8×10^4 cells mL⁻¹ in DMEM medium, supplemented with 10% (v/v) fetal calf serum and penicillin/streptomycin. After the cells were grown to confluence, the medium was replaced by a complex-containing DMEM/DMSO (8:1) and the cells were incubated further for 4 h. Then the cells were washed with DMEM medium, and extracted with 1 mL methanol. The complex content of each extract was determined spectrophotometrically. The data shown are mean values \pm standard deviation of three independent experiments.

Acknowledgements

This work was financially supported by the Ministry of Science and Technology (2013CB933801) and NNSFC (21390400, 21172228, 21273259, 21301182, and 81171633).

Notes and references

- (a) H. Lu, J. Mack, Y. Yang, Z. Shen, *Chem. Soc. Rev.*, 2014, **43**, 4778-4823; (b) S. A. Baudron, *Dalton Trans.*, 2013, **42**, 7498-7509; (c) N. Boens, V. Leen, W. Dehaen, *Chem. Soc. Rev.*, 2012, **41**, 1130-1172; (d) G. Ulrich, R. Ziesel, A. Harriman, *Angew. Chem.*, 2008, **120**, 1202-1219; *Angew. Chem. Int. Ed.*, 2008, **47**, 1184-1201; (e) A. Loudet, K. Burgess, *Chem. Rev.*, 2007, **107**, 4891-4932.
- A. Kamkaew, S. H. Lim, H. B. Lee, L. V. Kiew, L. Y. Chung, K. Burgess, *Chem. Soc. Rev.*, 2013, **42**, 77-88.
- (a) A. E. O'Connor, W. M. Gallagher, A. T. Byrne, *Photochem. Photobiol.*, 2009, **85**, 1053-1074; (b) M. R. Detty, S. L. Gibson, S. J. Wagner, *J. Med. Chem.*, 2004, **47**, 3897-3915.
- (a) S. Guo, L. Ma, J. Zhao, B. Küçüköz, A. Karatay, M. Hayvali, H. G. Yaglioglu, A. Elmalib, *Chem. Sci.*, 2014, **5**, 489-500; (b) J. Wang, Y. Hou, W. Lei, Q. Zhou, C. Li, B. Zhang, X. Wang, *ChemPhysChem.*, 2012, **13**, 2739-2747; (c) N. Adarsh, M. Shanmugasundaram, R. R. Avirah, D. Ramaiah, *Chem. Eur. J.*, 2012, **18**, 12655-12662.

- 5 (a) K. D. Mjos, C. Orvig, *Chem. Rev.* 2014, **114**, 4540-4563; (b) N. P. E. Barry, P. J. Sadler, *Chem. Commun.*, 2013, **49**, 5106-5131; (c) D. Gaynor, D. M. Griffith, *Dalton Trans.*, 2012, **41**, 13239-13257; (d) C. G. Hartinger, P. J. Dyson, *Chem. Soc. Rev.*, 2009, **38**, 391-401; (e) T. Gianferrara, I. Bratsos, E. Alessio, *Dalton Trans.*, 2009, **37**, 7588-7598.
- 6 B. W. Harper, A. M. Krause-Heuer, M. P. Grant, M. Manohar, K. B. Garbutcheon-Singh, J. R. Aldrich-Wright, *Chem. Eur. J.*, 2010, **16**, 7064-7077.
- 7 (a) Q. Zhou, W. Lei, J. Chen, C. Li, Y. Hou, X. Wang, B. Zhang, *Inorg. Chem.*, 2010, **49**, 4729-4731; (b) Q. Zhou, W. Lei, J. Chen, C. Li, Y. Hou, X. Wang, B. Zhang, *Chem. Eur. J.*, 2010, **16**, 3157-3165; (c) Y. Sun, L. E. Joyce, N. M. Dickson, C. Turro, *Chem. Commun.*, 2010, **46**, 2426-2428; (d) Y. Liu, R. Hammitt, D. A. Lutterman, R. P. Thummel, C. Turro, *Inorg. Chem.*, 2009, **48**, 375-385; (e) G. J. Ryan, S. Quinn, T. Gunnlaugsson, *Inorg. Chem.*, 2008, **47**, 401-403; (f) Y. Liu, R. Hammitt, D. A. Lutterman, R. P. Thummel, C. Turro, *Inorg. Chem.*, 2007, **46**, 6011-6021.
- 8 (a) Y. Chen, W. Lei, G. Jiang, Y. Hou, C. Li, B. Zhang, Q. Zhou, X. Wang, *Dalton Trans.*, 2014, **43**, 15375-15384; (b) M. A. Sgambellone, A. David, R. N. Garner, K. R. Dunbar, C. Turro, *J. Am. Chem. Soc.*, 2013, **135**, 11274-11282; (c) B. S. Howerton, D. K. Heidary, E. C. Glazer, *J. Am. Chem. Soc.*, 2012, **134**, 8324-8327; (d) S. Betanzos-Lara, L. Salassa, A. Habtemariam, O. Novakova, A. M. Pizarro, G. J. Clarkson, B. Liskova, V. Brabec P. J. Sadler, *Organometallics*, 2012, **31**, 3466-3479; (e) F. Barragán, P. López-Senín, L. Salassa, S. Betanzos-Lara, A. Habtemariam, V. Moreno, P. J. Sadler, V. Marchán, *J. Am. Chem. Soc.*, 2011, **133**, 14098-1410; (f) R. E. Goldbach, I. Rodriguez-Garcia, J. H. van Lenthe, M. A. Siegler, S. Bonnet, *Chem. Eur. J.*, 2011, **17**, 9924-9929; (g) S. J. Berners-Price, *Angew. Chem.*, 2011, **123**, 830-831; *Angew. Chem. Int. Ed.*, 2011, **50**, 804-805; (h) N. J. Farrer, J. A. Woods, L. Salassa, Y. Zhao, K. S. Robinson, G. Clarkson, F. S. Mackay, P. J. Sadler, *Angew. Chem.*, 2010, **122**, 9089-9092; *Angew. Chem. Int. Ed.*, 2010, **49**, 8905-8908; (i) S. Betanzos-Lara, L. Salassa, A. Habtemariam, P. J. Sadler, *Chem. Commun.*, 2009, 6622-6624.
- 9 (a) A. Naik, R. Rubbiani, G. Gasser, B. Spingler, *Angew. Chem.*, 2014, **126**, 7058-7061; *Angew. Chem. Int. Ed.*, 2014, **53**, 6938-6941; (b) J. Suryadi, U. Bierbach, *Chem. Eur. J.*, 2012, **18**, 12926-12934.
- 10 (a) A. M. Lifschitz, C. M. Shade, A. M. Spokoyny, J. Mendez-Arroyo, C. L. Stern, A. A. Sarjeant, C. A. Mirkin, *Inorg. Chem.*, 2013, **52**, 5484-5492; (b) T. Lazarides, T. M. McCormick, K. C. Wilson, S. Lee, D. W. McCamant, R. Eisenberg, *J. Am. Chem. Soc.*, 2011, **133**, 350-364; (c) Y. Zhong, L. Si, H. He, A. G. Sykes, *Dalton Trans.*, 2011, **40**, 11389-11395; (d) A. A. Rachford, R. Ziessel, T. Bura, P. Retailleau, F. N. Castellano, *Inorg. Chem.*, 2010, **49**, 3730-3736; (e) M. Galletta, F. Puntoriero, S. Campagna, C. Chiorboli, M. Quesada, S. Goeb, R. Ziessel, *J. Phys. Chem. A*, 2006, **110**, 4348-4358.
- 11 Q. Zhou, W. Lei, Y. Hou, Y. Chen, C. Li, B. Zhang, X. Wang, *Dalton Trans.*, 2013, **42**, 2786-2791.
- 12 (a) C. Hadjur, A. Jeunet, P. Jardon, *J. Photochem. Photobiol. B*, 1994, **26**, 67-74; (b) Y. Lion, M. Delmelle, A. Van De Vorst, *Nature*, 1976, **263**, 442-443.
- 13 R. H. Young, K. Wehrly, R. L. Martin, *J. Am. Chem. Soc.*, 1971, **93**, 5774-5779.
- 14 A. A. Abdel-Shafi, P. D. Beer, R. J. Mortimer, F. Wilkinson, *J. Phys. Chem. A*, 2000, **104**, 192-202.
- 15 W. Wu, H. Guo, W. Wu, S. Ji, J. Zhao, *J. Org. Chem.*, 2011, **76**, 7056-7064.
- 16 (a) A. M. Pyle, J. P. Rehmman, R. Meshoyrer, C. V. Kumar, N. J. Turro, J. K. Barton, *J. Am. Chem. Soc.*, 1989, **111**, 3051-3058; (b) D. S. Raja, N. S. P. Bhuvanesh, K. Natarajan, *Inorg. Chem.*, 2011, **50**, 12852-12866.
- 17 P. R. Ogilby, *Chem. Soc. Rev.*, 2010, **39**, 3181-3209.
- 18 (a) B. Yu, C. Ouyang, K. Qiu, J. Zhao, L. Ji, H. Chao, *Chem. Eur. J.*, 2015, **21**, 3691-3700; (b) B. Yu, Y. Chen, C. Ouyang, H. Huang, L. Ji, H. Chao, *Chem. Commun.*, 2013, **49**, 810-812; (c) X. Dong, X. Wang, Y. He, Z. Yu, M. Lin, C. Zhang, J. Wang, Y. Song, Y. Zhang, Z. Liu, Y. Li, Z. Guo, *Chem. Eur. J.*, 2010, **16**, 14181-14189.
- 19 F. H. Case, E. Kofit, *J. Am. Chem. Soc.*, 1959, **81**, 905-906.
- 20 J. G. Wang, Y. J. Hou, W. H. Lei, Q. X. Zhou, C. Li, B. W. Zhang, and X. S. Wang, *ChemPhysChem.*, 2012, **13**, 2739 – 2747.
- 21 M. Kepczynski, R. P. Pandian, K. M. Smith, B. Ehrenberg, *Photochem. Photobiol.*, 2002, **76**, 127-134.
- 22 (a) M. T. Carter, M. Rodriguez, A. J. Bard, *J. Am. Chem. Soc.*, 1989, **111**, 8901-8911; (b) R. B. Nair, E. S. Teng, S. L. Kirkland, C. J. Murphy, *Inorg. Chem.*, 1998, **37**, 139-141.